Separation and Purification Technology 233 (2020) 116059

Contents lists available at ScienceDirect

Separation and Purification Technology

journal homepage: www.elsevier.com/locate/seppur

Adsorption of Ce^{3+} and Nd^{3+} by diglycolic acid functionalised electrospun polystyrene nanofiber from aqueous solution

Omoniyi Pereao[a,*], Katri Laatikainen[b], Chris Bode-Aluko[a], Iurii Kochnev[c], Olanrewaju Fatoba[a], A.N. Nechaev[c], Leslie Petrik[a]

[a] Environmental and Nanoscience Research Group, University of the Western Cape, P.B. X17, Bellville 7535, South Africa
[b] Lappeenranta-Lahti University of Technology, Laboratory of Computational and Process Engineering, P.O. Box 20, FI-53851 Lappeenranta, Finland
[c] Flerov Laboratory of Nuclear Reactions, Joint Institute for Nuclear Research, 141980 Dubna, Russia

ARTICLE INFO

Keywords:
Polystyrene, rare-earth elements
Diglycolic acid
Adsorption
Nanofiber, selectivity

ABSTRACT

Highly selective and stable ligands with fast kinetics for rare earth element extraction are not well developed. Durable attachment of ligands to the support would make regeneration possible. Polystyrene nanofiber supports (PS-nF) were prepared using the electrospinning method. Thereafter, PS-nf were chemically modified with diglycolic anhydride (DGA) to produce novel electrospun polystyrene diglycolic acid nanofiber (PS-DGAnf) adsorbents. The immobilisation reaction proceeded via an electrophilic aromatic substitution of the ligand onto the PS nanofiber. The maximum gravimetric loading of DGA on PS nanofiber was 0.827 g g^{-1}. The unmodified and modified nanofibers were characterised by ATR-FTIR, HR-SEM, BET and TGA. After optimising pH, time and concentration, the equilibrium adsorption and binding kinetics of cerium (Ce^{3+}) and neodymium (Nd^{3+}) ions on the nanofibers surface were examined at pH 6. The adsorption capacity of PS-DGAnf for Ce^{3+} and Nd^{3+} at pH 6.0 was 152.5 mg g^{-1} (1.09 mmol/g) and 146.2 mg g^{-1} (1.01 mmol/g) respectively. Selectivity of Ce^{3+} over Ni^{2+}, Co^{2+} and Sr^{3+} was also studied at pH 6. The amount of Ce^{3+} adsorbed even in the presence of interfering ions was 100.3 mg g^{-1}, which was only a little lower than 119.4 mg g^{-1} obtained in a single ion solution. The rapid adsorption kinetics of Ce^{3+} and Nd^{3+} ions were achieved within 15 mins. The desorption and regeneration was carried out with 1 M nitric acid and the developed PS-DGAnf adsorbent could be reused for 4 cycles without any substantial loss to its adsorption abilities.

1. Introduction

Rare earth elements (REEs) have received increased consideration in recent decades, due to their distinctive properties and diverse applications in modern technologies, particularly in the nuclear fuel control, metallurgy, and ceramic industry [1,2]. Significant amounts of cerium and cerium oxide concentrates are used in glass-polishing applications and many cerium compounds have found important uses in biomedical applications [3] while neodymium, being the first triad of the lanthanide group, is illustrative for most of the valued REEs which are used in steel modifiers, optical filters, electronics components, superalloys, hydrogen storage and artistic glasses. Several hydrometallurgical techniques exist for the recovery and separation of REEs from aqueous solutions and these include adsorption, precipitation, ion exchange and solvent extraction [2,4,5], but disadvantages, such as the huge volume of chemical reagents needed, sludge generation, poor selectivity, and ineffective recovery from low metal concentrations [6], make obtaining the requisite rare earth metal purity very difficult.

The use of adsorbents and resins for removing or extracting rare earth metals from aqueous solutions was reported [7,8], and ligands comprising of the glycolamic acid group have been developed for REE removal. Results have indicated selectivity for the removal and recovery of REEs [9]. Diglycolic amic acid is comparable to diglycolic acid and well suited as task specific ligands capable of the removal of lanthanides [10], due to an etheric oxygen atom and two carbonyl groups as functional groups. Rare earth elements recovery using this ligand is now being reported [11,12]. In all these studies, ligands comprising of glycol amic acid exhibited very selective and effective extraction of REEs from mixtures of other diverse metals. Adsorbents comprising of glycol amic acid were utilised for scandium (Sc) separation and reported to preferentially extract Sc from a mixture [6]. Modification of *Escherichia Coli* (E. coli) through the succinylation of E. coli amine groups with the diglycolic amic acid ligand indicated high affinity to REEs [13]. Elastic diglycolic amic acid modified chitosan

* Corresponding author.
E-mail addresses: pereaokola@gmail.com, opereao@uwc.ac.za (O. Pereao).

https://doi.org/10.1016/j.seppur.2019.116059
Received 9 March 2019; Received in revised form 21 August 2019; Accepted 10 September 2019
Available online 10 September 2019
1383-5866/

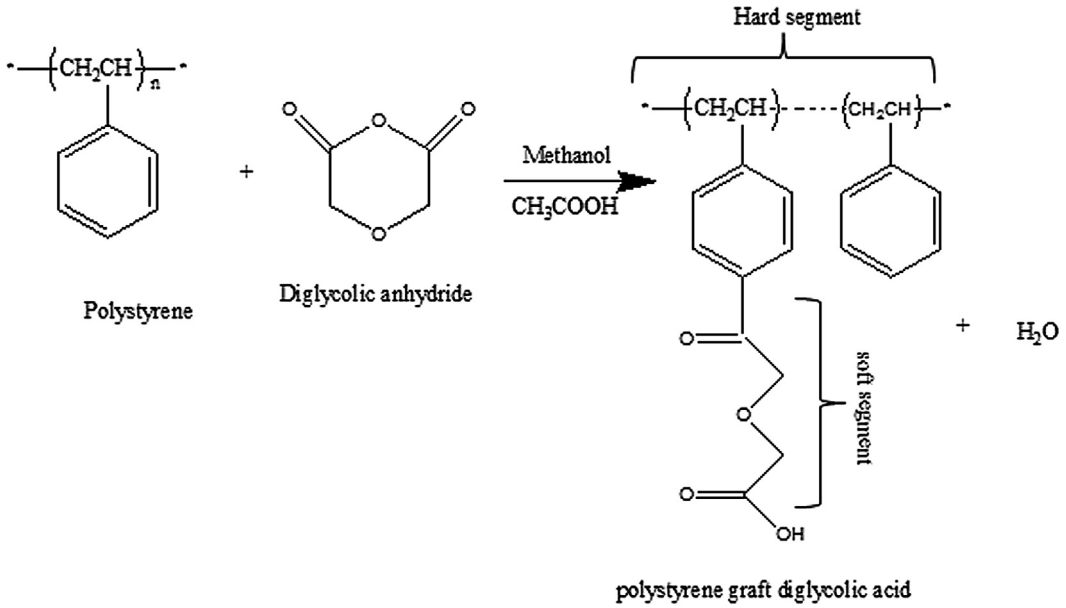

Scheme 1. Modification of PS nanofiber with DGA chelating ligand.

sponges were applied as adsorbents for the removal of REEs and reported to have fast adsorption kinetics [14]. The need for suitable supports in designing a practical adsorbent for the recovery of REE are being investigated and some research on the adsorption of REEs using diglycol amic acid immobilised using different supports was published with varied results [15,16].

Nanofibers have high interfiber porosity with excellent interconnectivity, high surface area to volume ratios, layer thinness, low basis weight, controllable thickness of the electrospun scaffold, good structural stability as well as being cost effective, which make them promising materials [17]. Nanofibers can be functionalised with suitable ligands in a viable and cost effective manner [18] and these functionalised nanofibers can provide an effective, high surface area support which could be useful for waste water treatment and purification [19]. Electrospinning is a feasible technique that can be used to fabricate nanofibers of diameters in the range of 40–500 nm with the use of electrostatic forces [20,21]. Electrospun nanofibers are produced from numerous natural or synthetic polymers, or some blends or hybrids of both types of polymers [22]. Polystyrene (PS) is a versatile synthetic polymer support, due to the large number of ligands that can be covalently bound to it [23]. Because of its outstanding physical and reactive properties, chemical resistance, ease of electrospinning, good mechanical properties and low cost, PS is well studied, but it cannot efficiently adsorb individual metal ions [24].

In this study, the surface of PS nanofibers were modified chemically using diglycolic acid chelating ligands and their effectiveness in aqueous solutions for the recovery of Ce^{3+} or Nd^{3+} was assessed by performing batch adsorption studies. The dependence of factors including contact time, pH and equilibrium concentration on Ce^{3+} and Nd^{3+} adsorption efficiency as well as selectivity was studied. The desorption of REEs from the loaded PS-DGAnf and the regeneration of the functional fibers using nitric acid was determined.

2. Experimental

2.1. Materials

Polystyrene (Mw ~ 192,000), diglycolic anhydride (90%), neodymium(III) nitrate hexahydrate (99.9%), cerium(III) nitrate hexahydrate (99.99%), N,N-dimethylformamide (DMF) (≥99.8%), methanol (≥99.9%), acetic acid (100%), tetrahydrofuran (THF) (≥99.0%), HNO_3 (69%), NaOH (99.9%), strontium nitrate (> 99.0%) were all purchased from Sigma-Aldrich (South Africa), $NiSO_4{\cdot}6H_2O$ (98%), and $CoSO_4{\cdot}7H_2O$ (97.5%) were purchased from Merck Chemicals. Deionised water was used throughout this work. All the reagent grade chemicals were used without any further purification.

2.2. Electrospinning

Electrospinning was performed using an infusion pump (Harvard Apparatus 33 Twin Syringe Pump) and applied voltages were driven by a high voltage power supply. The PS was dissolved in a 10 mL dimethylformamide and tetrahydrofuran (DMF:THF) (4:1 v/v) solvent system. The mixture was agitated by a magnetic stirrer for 12 h to achieve a consistent and homogenous solution. The attained viscous PS solution was thereafter loaded into a 10 mL glass syringe, and mounted on the programmable infusion pump. The electrospinning procedure was carried out under ambient conditions, and nanofibers were collected on aluminium foil as a non-woven nanofiber mat. The fiber diameter was evaluated using Image J® software. For this study, PS concentration was investigated, at varied concentration of 10, 15, 20, 25 or 30 wt% PS polymer in DMF:THF (4:1 v/v) with flow rate (1 mL/h), collector distance (17 cm) and applied voltage (20 kV) as fixed parameters. The applied flow rate was also changed from 0.2, 0.4, 0.8 to1.0 mL/h using a fixed voltage of 20 kV, 15 wt% PS polymer in DMF:THF (4:1 v/v) solution concentrations and a fixed tip to collector distance of 17 cm.

2.3. Surface modification of PS nanofibers

The experiments were undertaken according to previously reported chemical grafting procedures [25–27]. The reaction is an acid-catalysed process using acetic acid. First, a suitable amount of diglycolic anhydride was added to 10 mL of 5% (v/v) aqueous acetic acid solution in 40 mL methanol (99.9%) and the reaction mixture was mechanically stirred for 30 min. To functionalise the synthesised electrospun PS with DGA, fiber mats were inserted into the stirred solution and the temperature was slowly raised to 43 °C under reflux with further constant stirring for 4 h (Scheme 1).

Typically, PS electrospun nanofibers were cut into 5 cm by 5 cm square shapes weighing 0.109 g and immersed in a mixture of different ligand concentration range of 1 to 4 g diglycolic anhydride in 10 mL of

5% (v/v) aqueous solution of acetic acid in 40 mL methanol (99.9%) and shaken for 4 h at 43 °C in a beaker. PS nanofibers were tested at different reaction times between 1 and 4 h in 3 g of diglycolic anhydride containing solution under the same conditions and after the reactions, the PS-DGAnf samples were washed in deionised water to remove the residual salts and any unreacted ligand and the fibers were air-dried overnight. Stability experiments were performed to determine if the optimised material (PS-DGAnf) obtained can withstand short term contact with 1 M HNO_3 as regenerant for 1 h to mimic the conditions that would be used for batch desorption experiments. The fiber samples were then washed with deionised water and air dried. The modification reaction was carried out using triplicate samples for each considered parameter.

2.4. Analytical methods

Thermo Scientific-Nicolet iS10 Fourier Transform Infrared Spectrophotometer (FT-IR) equipped with diamond Attenuated Total Reflectance (ATR) was used to record spectra in the range of 4000 – 650 cm^{-1} to assess and identify the specific functional groups on the nanofiber surfaces before and after modification. The morphology of the nanofibers was investigated using the Zeiss Gemini Auriga high resolution scanning electron microscope (HRSEM) fitted with a CDU-lead detector using 25 kV with tungsten filament. Nanofiber diameters were evaluated using Image J® analysis software. The nitrogen adsorption/desorption (Brunauer-Emmett-Teller (BET)) isotherms were assessed by using a Micromeritics Tristar porosity and surface area analyser fitted with a Micromeritics flowprep 060 sample degas system and were measured at −196 °C. Thermal behaviour of the fibers and stability of the immobilised ligands were investigated by thermogravimetric analyser (TGA) using STA 6000 (Perkin-Elmer Instrument Model, USA) under nitrogen. The metal ion concentration in solution before and after the adsorption experiments was acidified with 2% HNO_3 and determined by Inductively Coupled Plasma-Optical Emission Spectroscopy (ICP-OES). The instrument used for determining the metal ion concentrations was a Varian Radial ICP-OES coupled with a High Matrix Introduction (HMI) accessory.

2.5. Batch adsorption

The surface-modified adsorbents PS-DGAnf were applied in batch studies to investigate their performance in the removal of two rare earth metals (Ce^{3+} and Nd^{3+}) from solution. For each REE, 0.0075 g of PS-DGAnf was immersed in a vial of the single metal ion solution containing 10 mL of Ce^{3+} or Nd^{3+} (100 mg/L) respectively. The pH was adjusted in the range 1 to 6 by using NaOH or HNO_3. It was then shaken for a period of 2 h using an agitation speed of 200 rpm until equilibration was reached and the solution was then filtered with 20–25 µm filters (Whatman® qualitative filter paper, Grade 4) before analysis. The ICP OES was used for the determination of the REEs concentration in the aqueous stock, and in extracted solutions. The changes between the initial and final concentration of the solutions were considered to be the concentration of metal ion adsorbed. Initial concentration was changed from 60 to 180 mg/L at pH 6.0 for studying the adsorption isotherms of Ce^{3+} or Nd^{3+} on the surface of functionalised PS-DGAnf. Contact times were changed from 1 to 60 min at pH 6.0 to evaluate the efficiency of the adsorption kinetics. The initial and final readings were then calculated using Eq. (1).

$$q_e = \frac{(C_O - C_e)V}{m} \tag{1}$$

For aqueous phase adsorption, it is a practice to calculate distribution coefficient (Kd) [28] defined using Eq. (2),

$$K_d = \frac{C_o - C_e}{C_e}\left(\frac{V}{m}\right) \tag{2}$$

where: q_e is the metal ions adsorbed by the nanofiber adsorbent (mg g^{-1}). M and V are adsorbent weight and solution volume while C_0 and C_e are the initial and final equilibrium solution concentrations of metal ions. To confirm the actual concentration of working solutions, negative controls (with no adsorbent) were concurrently carried out to determine the metal ion loss during the adsorption due to the glassware. The experiments were generally carried out at 22 ± 1 °C and the entire batch experiments were performed in duplicate.

2.6. Desorption and reusability studies

To examine the feasibility of regenerating PS-DGAnf, desorption studies were performed using 1 M HNO_3 for 1 h. The regenerated PS-DGAnf were then washed about 3 times in 10 mL portions of ultrapure water and dried on a filter using vacuum suction before reuse. The regenerated nanofiber mats were dried at 40 °C overnight. This regeneration was repeated three times under the same adsorption and desorption conditions to determine how many regeneration cycles were possible. The desorption efficiency was calculated using Eq. (3).

$$D_E = \frac{\mathrm{cx}v}{\mathrm{q}x m} \times 100\% \tag{3}$$

where C (mg/L) is the concentration of adsorbates in the desorption solution, q (mg g^{-1}) is the amount of adsorbate adsorbed on the nanofiber before the desorption experiment, V is the volume of the desorption solution, and m (mg) the amount of the adsorbent used in the desorption experiments.

2.7. Selective adsorption of Ce(III) and Nd(III) onto PS-DGAnf.

The metal selectivity of PS-DGAnf was examined in 15 mL plastic vials containing 10 mL of aqueous solution of various metal ions (Ce^{3+}, Co^{2+}, Ni^{2+} and Sr^{2+}) using equal concentrations of 100 mg/L each and the nanofiber adsorbent (0.0075 g) was immersed into the solution. The fiber samples in the vials were equilibrated in a shaker operated at 200 rpm for 1 h in pH 6.0. The concentration of the various metal ions initially in solution and after adsorption was determined. The amount of metal ions absorbed on the nanofiber sample at adsorption equilibrium (qe, mg g^{-1}) was calculated according to Eq. (1), and the selective coefficient of $K_{REE/M}$ was calculated using Eq. (4)

$$K^{REE_M} = \frac{q_{REE} * C_M}{q_M * C_{REE}} \tag{4}$$

where q_{eREE} and q_{eM} was the amount of REE ion and metal ions adsorbed onto PS-DGAnf at equilibrium.

3. Results and discussion

3.1. Electrospinning

The electrospinning effects on the solution polymer concentration and flow rate on the morphology and fiber diameter of polystyrene nanofibers were studied. The fibers produced at the low polymer weight percentage of 10 wt% showed that the bead-on-string morphology turned into blobs of polymer but by increasing the concentration of PS in solution, a morphological transformation of the beaded fibers to more cylindrical fibers with average fiber diameters ranging from 350 nm to 900 nm at a higher concentrations were obtained as presented in Fig. 1 and the fiber diameter further used for this study was in the range of 392 nm. The fiber diameter increased due to a raise in polymer concentration and to insufficient stretching or elongation of the ejected jets with higher viscosity of the electrospinning solution. The beads on strings and bead formation in the electrospinning process was ascribed to lower viscosity, higher surface tension, and the low polymer concentration of the polymer solution [18,29].

Different flow rates were also investigated at 0.2, 0.4, 0.8 and

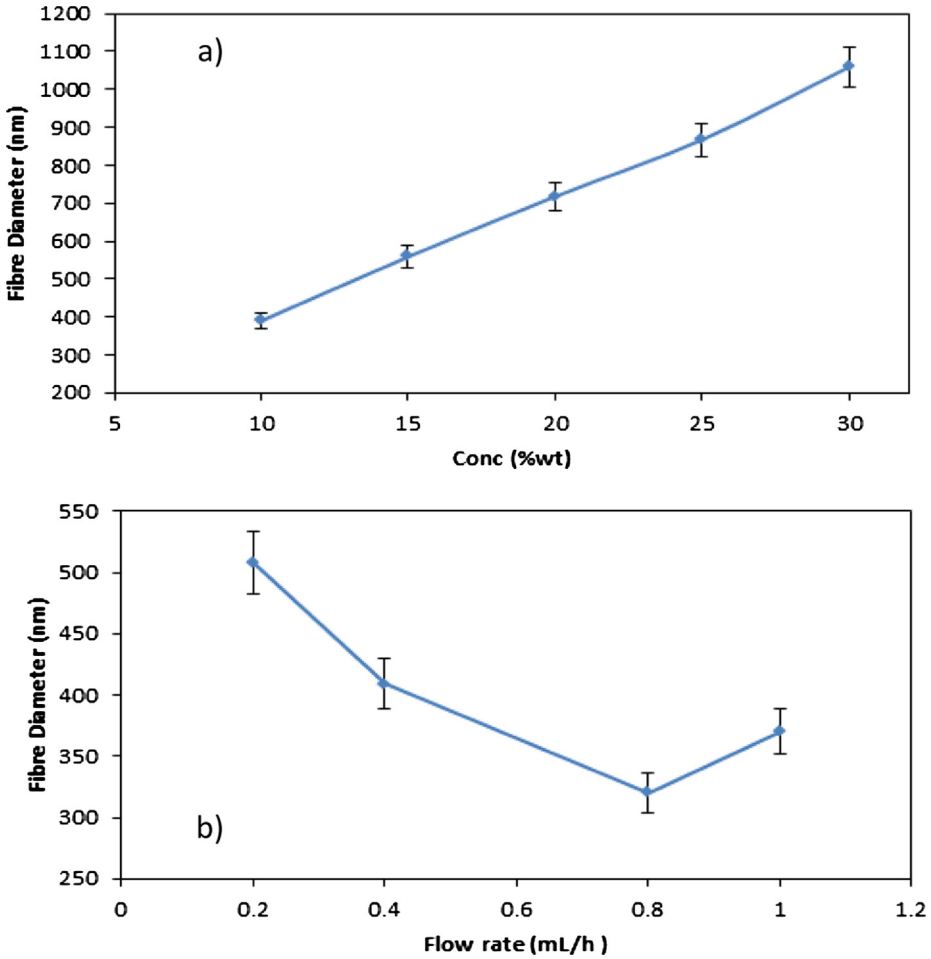

Fig. 1. Trend of the effect of (a) PS solution concentration (flow rate-1 mL/h; distance-17 cm; voltage-20 kV) (b) flow rate (voltage-20 kV, conc-15 wt.%; distance-17 cm) on the fiber diameter.

1.0 mL/h using fixed polymer concentration of 15 wt%; applied electrostatic potential of 20 kV and collection distance of 17 cm. The effect of flow rate on fiber diameter for polystyrene (PS) showed a decrease of fiber diameter (500 to 350 nm) from 0.2 mL/h up to an optimum of 0.8 mL/h flow rate, but there was an increase in fiber diameter when the flow rate was increased to 1.0 mL/h as depicted in Fig. 1(b). The fibers produced at the high flow rate of 1.0 mL/h showed the bead-on-string morphology and an increased fiber diameter while too low flow rate (0.2 mL/h) of the spinning solution caused obstructions to the needle nozzles when hanging droplets appeared on the tip of the needle and dried up, thus sealing the nozzle with the solidified polymer residue. The optimal solution flow rate used for fabricating PS nanofibers was determined to be 0.8 mL/h and 15 wt% PS concentrations in DMF:THF (4:1 v/v) were suitable for fabricating nanofibers with well-defined structure.

3.2. Surface modification and morphology of PS-DGAnf

To examine and confirm the effective synthesis of PS-DGAnf, various characterisation techniques were used. The as-made and modified PS-DGAnf obtained after DGA functionalising at different reaction times of 2, 3, and 4 h was studied by HRSEM and shown in Fig. 2. The PS nanofiber mats obtained are very similar with uniform surface morphology to that of the as-made PS fibers. However, there is a slight increase in fiber diameter from 392 nm to 462 nm, 475 nm and 485 nm respectively with increased DGA reaction time during fiber modification. The smooth fiber structures were not altered due to DGA attachment, and 3 h was selected because this afforded sufficient time for the modification without denaturing the nanofiber.

The effect of the ligand concentration on the modification of PS-DGAnf was investigated and showed smooth fibers with no beads or beads-on-strings prior to modification and after modification but an increase in fiber diameter from 392 nm to 456 and 481 nm respectively for 2 and 3 g DGA ligand concentration. 3 g DGA was selected as the characteristic FTIR bands and peaks for DGA were already present as shown in Fig. 3(b). Increasing DGA concentration may result in a waste of ligands and anchoring of the ligand showed no morphological changes or damage to the PS nanofibers after the functionalisation steps. The known poor mechanical characteristics of PS adsorbents may make them susceptible to impairment [30] but as revealed from the HRSEM, the fibers remained smooth and still retained their nanofiber structure up to 4 h of functionalisation time. Physical examination showed no mechanical damage to the fiber.

3.3. Characterisation of PS-DGAnf

The effective functionalisation of PS nanofiber with the diglycolic acid moiety was confirmed by FT-IR spectroscopy. As depicted in Fig. 3, the FTIR spectrum in Fig. 3a identified aromatic C-H bond stretching vibrations at 1601; 1493; 1453 cm^{-1}, deformation of the aromatic ring CH_2 and C=C at 1026 $cm^{-1;}$ 756 cm^{-1} which confirmed the presence of the main characteristic peaks of PS. Fig. 3b depicts the FTIR spectrum of the two C=O groups of DGA band at 1800–1700 cm^{-1} that is related to the stretching vibrations. The bands due to the scissoring vibrations of CH_2 groups are observed in the 1425 cm^{-1} range.

Fig. 3c depicts the spectra of the functionalised nanofibers and the

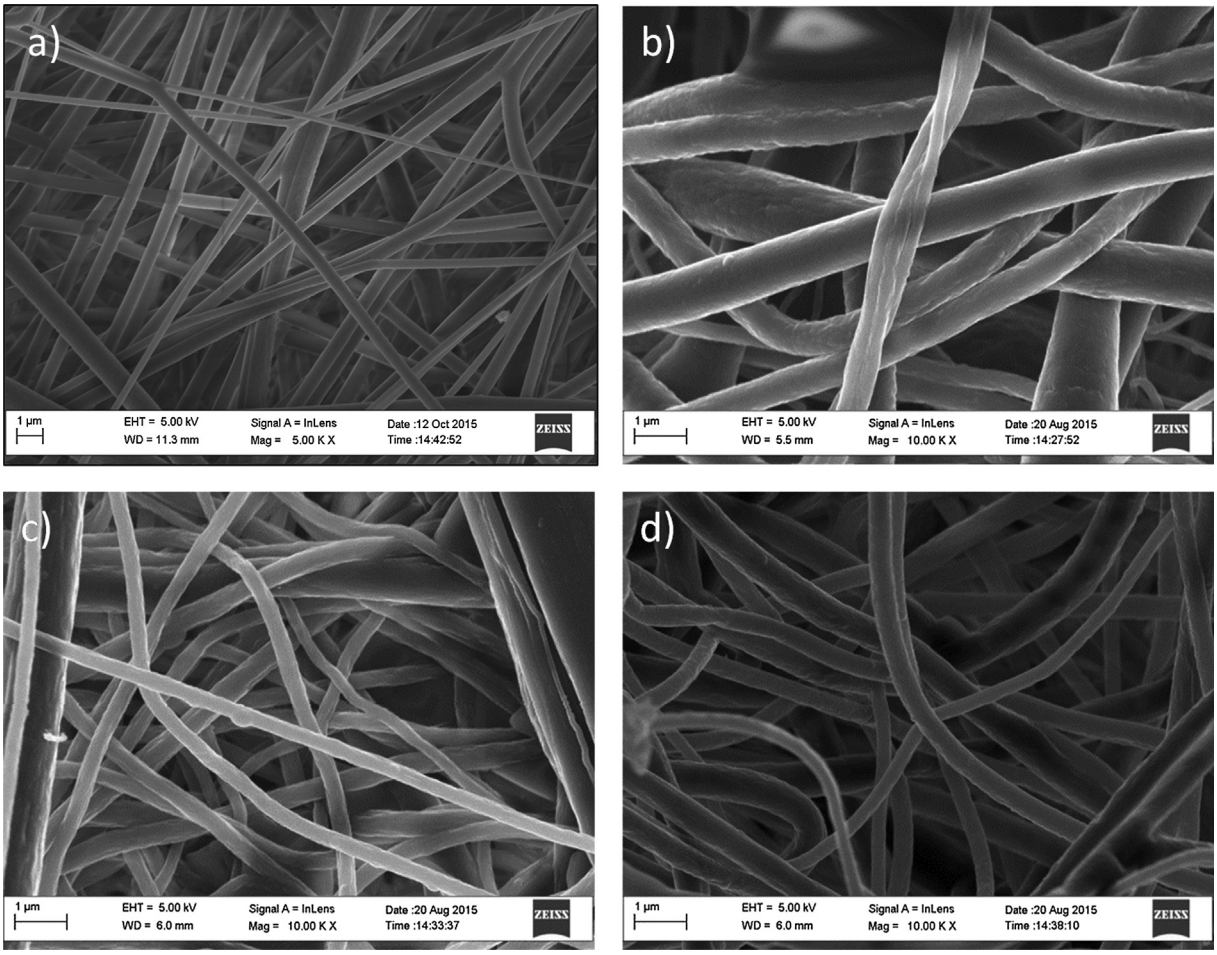

Fig. 2. SEM micrograph (a) pristine PS (b) PS-DGAnf at 2 h (c) PS-DGAnf at 3 h d) PS-DGAnf at 4 h (DGA conc −3 g; initial fiber weight −0.109 g).

presence of C=O groups on the PS polymer matrix. The carbonyl (−C=O) group stretching vibration peak at 1737 cm^{-1}, 1128 cm^{-1} and 1227 cm^{-1} confirmed the successful functionalisation of PS nanofiber with DGA while the $-CH_2$ bending peak at 1454 cm^{-1} of the polymer support confirmed the presence of PS backbone structure. The PS-DGAnf spectra exhibited a very strong peak at 1737 cm^{-1} that is representative of the C−O stretch. The adsorption band at 1227 cm^{-1} could possibly be allotted to the asymmetric stretching of the C−O and C−C bonds attached to the carbonyl carbon while the band at 1128 cm^{-1} may be due to vibrations relating to the two carbons and oxygen attached to the chain. PS-DGAnf was shaken in 1.0 M of HNO_3 for 1 h to mimic the conditions utilised for batch desorption testing. As shown in Fig. 3d, the peak positions and shapes were consistent with Fig. 3c (PS-DGAnf) after the nitric acid regeneration test. These results

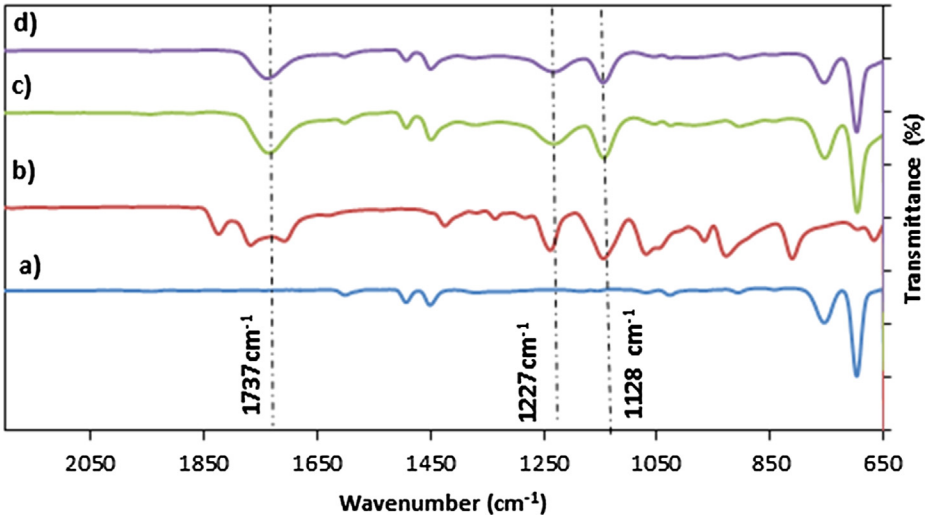

Fig. 3. FTIR spectra of a) Pristine PS, b) DGA and c) PS-DGAnf (time −240 mins; PS fiber weight −0.109 g; temp –43 °C; 5 mL acetic acid; 40 mL 99% methanol) d) regenerated-PS-DGAnf (Vol –10 mL; time −1 h; rpm –240; Conc −1.0 M of HNO_3).

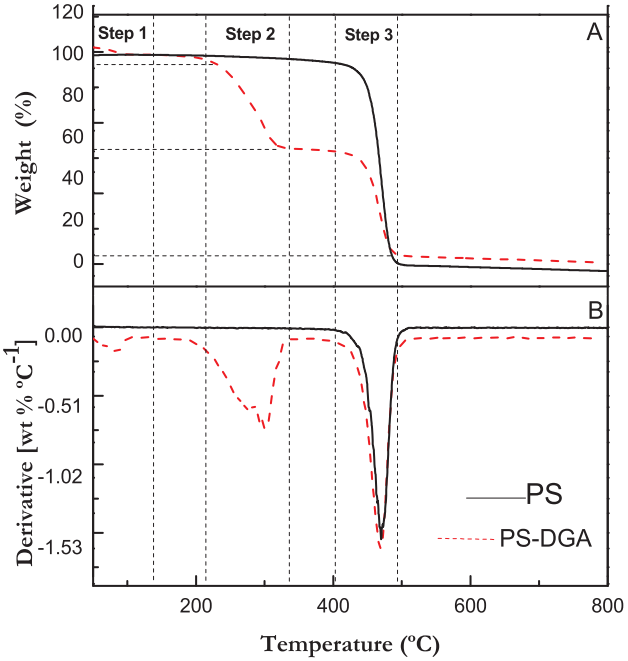

Fig. 4. (a) TGA profile (b) TGA derivatives of pristine PS and PS-DGAnf.

indicate that the chemical modification and structure of the PS-DGAnf were not adversely affected by any chemical destruction or degradation due to 1.0 M nitric acid after 1 h exposure.

The TGA thermograms weight loss curves of electrospun PS nanofibers showed that PS nanofibers (Fig. 4) only started losing their thermal stability at temperatures around 215 °C and were completely pyrolysed at 487 °C in two steps. However, the PS-DGAnf TGA thermograms showed loss of a small amount of mass at 80–100 °C due to the solvent used because oxygen-containing functional groups of DGA resulted in water adsorption and thus, some mass loss below 100 °C was expected. The second weight loss between 215 and 350 °C, corresponded to CO_2, CO, and steam released from the labile oxygen containing functional groups. The additional mass loss between 405 and 498 °C was ascribed to the degradation of more stable oxygen functionalities which was an indication of the independent decomposition of components (PS nanofiber; DGA functionalities) in the modified nanofiber adsorbent.

The TGA results showed good attachment of DGA onto PS. Thus, the TGA result confirmed that the surface of PS-DGAnf was successfully functionalised with DGA. PS and PS-DGAnf reached a char value of about 40.5 wt% at 500 °C. The amount of DGA adsorbed onto the PS nanofiber was gravimetrically determined by TGA and was estimated to be 0.827 g g^{-1}. This deduction was made from the TGA profile as shown in Fig. 4 using the mass of ligand immobilised per gram of PS-DGAnf. The N_2 BET adsorption–desorption characterisation in Fig. 5a depicts the N_2 adsorption–desorption isotherm for PS, showing a substantial uptake of nitrogen because of the capillary condensation in the range of 0.6 to 0.99 at relative pressure (P/P_0) which is indicative of multiform distribution of the interfiber pores. The BET surface area of PS-DGAnf (67.3 m^2/g) was higher than that of the pristine PS (41.3 m^2/g).

Fig. 5b shows that PS-DGAnf has a hysteresis loop at relative pressure which is > 0.8. This hysteresis loop Type H1 which is associated with porous materials that consist of compacts or agglomerates in fairly regular array and of approximately uniform spheres [31]. The average pore diameter between the as-made nanofibers was measured to be 8.86 nm in the range of 1–18 nm. The measured PS-DGAnf average pore diameter was 13.2 nm in the range of 6 to 23 nm. The average pore size between fibers of surface modified PS-DGAnf was higher than that of untreated nanofiber and could be associated with crosslinking between ligand and the nanofiber matrix and the creation of mesopores between adjacent nanofibers. The nitrogen adsorption–desorption isotherm for the PS-DGAnf may be assigned to a type V isotherm [32] and the porous structure and large specific surface area showed that the PS-DGAnf will have prospective applicability in adsorption or separation.

3.4. Batch adsorption studies

The feasibility of PS-DGAnf as adsorbent was demonstrated for the removal of rare earth metals, (Ce^{3+} and Nd^{3+}) from solution. The removal and extraction effectiveness can be studied by using several factors as described below. The pH experiment was manually adjusted to a pH ranging between 1 and 6 with 0.1 M HNO_3 or NaOH solution. In previous studies, precipitation was noticeable at a higher pH than 6 [33] due to the speciation of REEs. Therefore, this study was limited to a maximum pH of 6. The uptake of metals below pH 2 was limited due to proton attachment to the adsorption sites because under acidic conditions, the surface of PS-DGAnf was covered with H^+ ions which were in competition with the Ce^{3+} and Nd^{3+} ions adsorption upon the surface of the adsorbent.

Fig. 6 displays an initial low adsorption capacity of Ce^{3+} at very low pH values, since the active sites on PS-DGAnf are mostly protonated. But as the pH increases, the H^+ ions concentration decreased leading to less protonation and increased vacant sites available for metal ion adsorption. Nd^{3+} adsorption improved after pH 4 and increased rapidly up to pH 6 while Ce^{3+} adsorption started from pH 3 and increased gradually up to pH 6. The adsorption reached the maximum amount of 44.42 or 79.86 mg g^{-1} for Ce^{3+} or Nd^{3+} at pH 6, respectively. The pH of 6 was used to monitor the adsorption for Ce^{3+} or Nd^{3+} from synthetic aqueous solutions for subsequent adsorption studies in order to avoid metal hydroxide formation. The dependence of Ce^{3+} and Nd^{3+} adsorption on the increasing pH of the solution suggested that the carboxylic groups progressively formed carboxylate functions that can bind metal cations by chelation [34].

The PS-DGAnf adsorbent functionality with the large number of active sites was investigated for the interaction with Ce^{3+} or Nd^{3+} ions by testing the solution concentration to understand the adsorption capacity. The different initial concentrations of the metal ions investigated ranged from 60 to 180 mg/L while other factors, such as equilibration time, pH and adsorbent quantity, were kept constant. At a concentration of metal ion of 100 mg/L, there were sufficient sites for all the available metal ions, and on increasing the concentration, there was an increased adsorption up to 140 mg/L indicating enhanced capacity. The attained results indicated that binding efficiency increased together with increased metal ion concentrations up to 140 mg/L until the equilibrium was reached. As shown in Fig. 7, the equilibrium was reached at metal ion concentrations of between 140 and 180 mg/L because of the saturation of the available ligand binding sites present on the PS-DGAnf. This increase in uptake with a rise in concentration may be associated with the large surface area and the numerous vacant binding sites upon inter fibrous pores of the nanofibers. The high uptake capacities observed was mainly due to the specific interaction between the metal ion and the functional groups on the nanofiber surface since only a negligible amount of the target metal ions was adsorbed by pristine PS nanofibers (not shown). The maximum adsorption capacities of Ce^{3+} or Nd^{3+} ions on the PS-DGAnf were 152.0 or 144.0 mg g^{-1} respectively indicating that the available sites were fully occupied.

The adsorption isotherms were analysed by using Langmuir and Freundlich models [35,36] to interpret and elucidate the experimental data and matching parameters associated with the models are illustrated in Table 1. The maximum Langmuir adsorption capacities (q_e) for Ce^{3+} or Nd^{3+} were 152.5 mg g^{-1} (1.09 mmol/g) or 146.2 mg g^{-1} (1.01 mmol/g) respectively. This number is very close to the measured values of 152.1 mg g^{-1} (1.09 mmol/g) for Ce^{3+}; and 144.0 mg g^{-1}

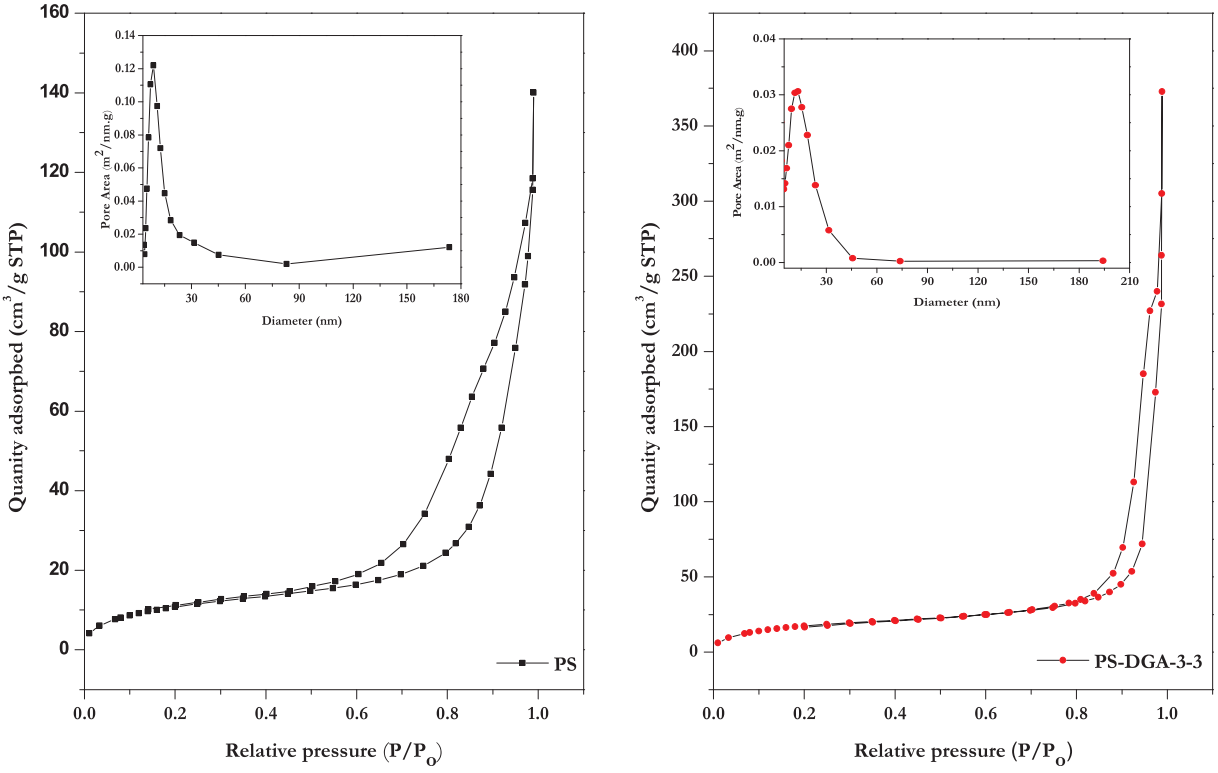

Fig. 5. N_2 adsorption–desorption isotherm for (a) PS and (b) PS-DGAnf. (Inset) Pore size distribution of PS and PS-DGAnf.

(0.998 mmol/g) for Nd^{3+} at the C_e of 140 mg/L, indicating the dependability of q_e value.

The correlation coefficient R^2 values for the Langmuir equation were 0.999 or 0.992 for Ce^{3+} or Nd^{3+} respectively which indicated that the Langmuir isotherm better fitted the experimental data than the Freundlich model and could better explain the Ce^{3+} or Nd^{3+} adsorption process. The Langmuir advocates 3 major situations such that (i) there is no inter-action between the monolayer of molecules (ii) the intermolecular attractive forces among the adsorbate molecules in the solution and the monolayer decreases significantly with distance, and (iii) the sorption of adsorbate molecules in neighbouring sites do not influence or impact the adsorption of other molecules in other adsorbing site [37], therefore, the Langmuir isotherm model suggest homogeneous binding sites on the surface of PS-DGAnf andalso allowed comparison with literature (Table 2).

The evidence provided by FTIR data showed that strong adsorption is likely involved in the interactions of Ce^{3+} or Nd^{3+} with multiple carbonyl groups on the nanofiber. Hence, the Ce^{3+} and Nd^{3+} adsorption tended to be homogeneous and showed monolayer coverage, because of the strong interactions between the surface functional groups of PS-DGAnf and Ce^{3+} and Nd^{3+} which is also consistent with the much higher Kd value (Fig. 8). The sorption properties of the nanofiber adsorbents for Ce^{3+} or Nd^{3+} were matched to the sorption capacities of alternative or commercial sorbents also fitted by the Langmuir model

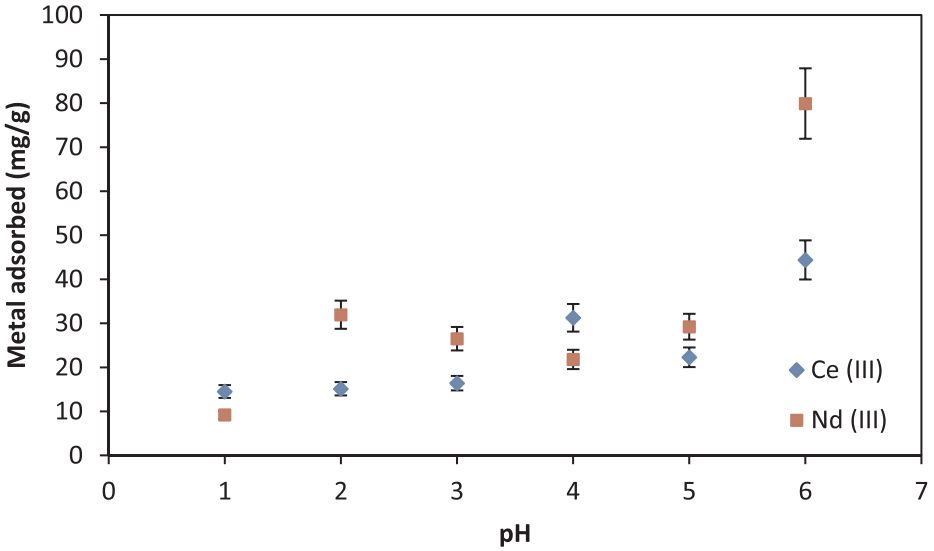

Fig. 6. Dependence of Nd^{3+} and Ce^{3+} adsorption on pH of solution using PS-DGAnf (contact time −120 min; Ce^{3+} or Nd^{3+} concentration −100 mg/L; adsorbent dosage −0.0075 g/10 mL).

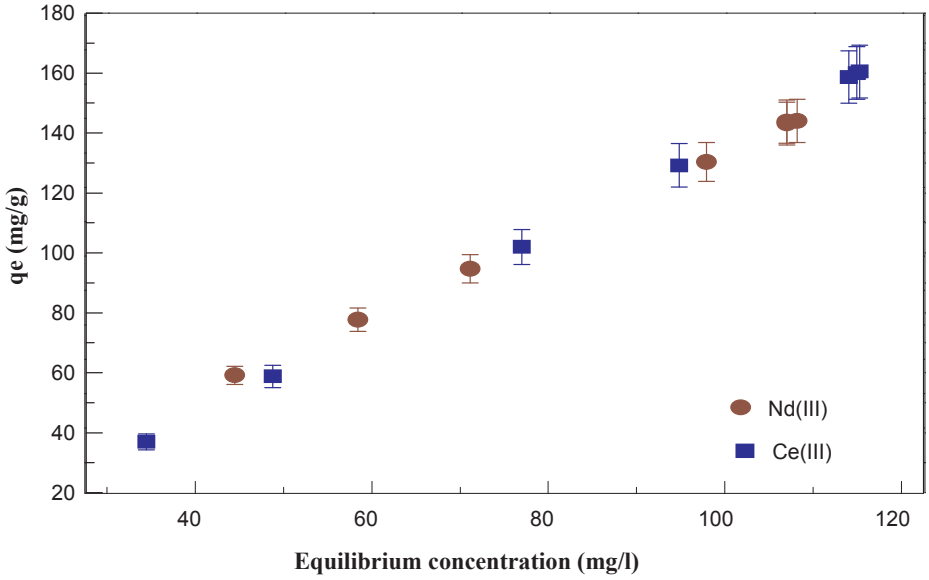

Fig. 7. Adsorption isotherm models fitted to experimental adsorption of (a) Ce^{3+} (b) Nd^{3+} onto PS-DGAnf (contact time −90 min; initial concentrations −60–180 mg/L; pH −6; adsorbent dosage −0.0075 g/10 mL).

Table 1
Parameters obtained from the plot of Langmuir and Freundlich isotherms for Ce^{3+} or Nd^{3+} adsorption using PS-DGAnf.

			Langmuir isotherm		Freundlich isotherm		
	qe (exp)mg g^{-1}	R^2	b1 (L/mg)	qm (mg g^{-1})	R^2	n	kf [(mg g^{-1}) (mg/L)1/n]
Nd^{3+}	144.0	0.992	0.00356	146.2	0.816	2.15	14.6
Ce^{3+}	152.1	0.999	0.00013	152.5	0.988	1.12	2.10

which are typically adopted in the studies of absorbents for the extraction of REEs. Due to the different bulk and surface properties, it was difficult to perform a fair comparison. However, the data in Table 2 still provided useful information especially on the order of magnitude of removal of the metal ions.

The adsorption capacity (q_e) value of PS-DGAnf is competitive with and out performs other absorbents when compared with the previously reported adsorbents. Even though some materials such as phosphoric acid functionalised adsorbents [43], calcium alginate–poly glutamic acid [42], chitosan/polyvinyl alcohol/3-mercaptopropyltrimethoxysilane beads [45] or impregnated alginate microcapsules [44] showed considerably higher sorption levels than those achieved with PS-DGAnf, their modification and synthesis was more complex. These new nanofiber adsorbents have improved sorption capacities and rapid kinetics (Section 3.5) when compared to other similar conventional adsorbents, and were made using a simple, one-step grafting procedure to obtain the functionalised adsorbents. Ogata et al [16] clarified the adsorption mechanism of immobilized diglycolic amic acid ligands by showing that adsorbents with diglycolic amic acid ligands adsorb REE ions via three oxygen atoms and that the tridentate chelation conferred high selectivity for REE ions.

The REE cations are strong Lewis acids and easily coordinate nucleophiles to form stable complexes and they show a clear tendency towards oxygen donors which is advantageous for their efficient extraction. The derivatives of DGA are used for the selective extraction of REEs from aqueous solutions, because they are recognised as effective and size selective binders of trivalent f-elements [49]. The structural analysis of complexes bearing the DGA ligands shows that REEs bind traditionally in a tridentate fashion, where each metal ion is coordinated by the three oxygen atoms of DGA-type ligands. The lanthanide ions (e.g., La, Nd, Ce) are sterically saturated in their nine-coordinate geometry with three DGA ligands [50]. Therefore, by the right tailoring of chemically similar chelating ligands and their grafting on solid supports, it is possible for functional materials to exhibit selective affinities for smaller or larger ions [51,52].

The distribution coefficient values as a function of initial

Table 2
Sorption capacities of different sorbents in comparison to PS-DGAnf.

Sorbent	Metal	pH	time (h)	Adsorption capacity (mg g^{-1})	Reference
Arthrospira cyanobacteria	Ce^{3+}	5.5	1	38.2	[38]
Hybrid nano-material	Ce^{3+}	5	3.5	130	[39]
Amino Phosphate Nano TiO_2	Ce^{3+}	6	1.5	21.39	[40]
Aminomethylphosphonic acid modified chitosan	Nd^{3+}	5	7	30.32	[41]
Calcium alginate–poly glutamic acid	Nd^{3+}	3.5	24	237.99	[42]
Phosphoric acid on silica matrix	Nd^{3+}	6	24	160	[43]
Aspartic acid grafted Cellulose	Nd^{3+}	5	3	81.2	[34]
Extractant impregnated alginate microcapsules	Nd^{3+}	4	20	149.3	[44]
chitosan/polyvinyl/Alcohol/3-mercapto Beads	Ce^{3+}	5	6	251.41	[45]
EDTA and DTPA-functionalised chitosan	Nd^{3+}	4	3	7477	[46]
Phosphorous functionalized nanoporous carbon	Nd^{3+}	–	1	335.5	[47]
4-dodecyl-6-((4-(hexyloxy)phenyl)diazenyl) benzene-1,3-diol mesoporous silica nano-composite	Ce^{3+}	2.5	2	150.37	[48]
PS-DGAnf	Nd^{3+}	6	0.4	146.2	This work
PS-DGAnf	Ce^{3+}	6	0.4	152.5	This work

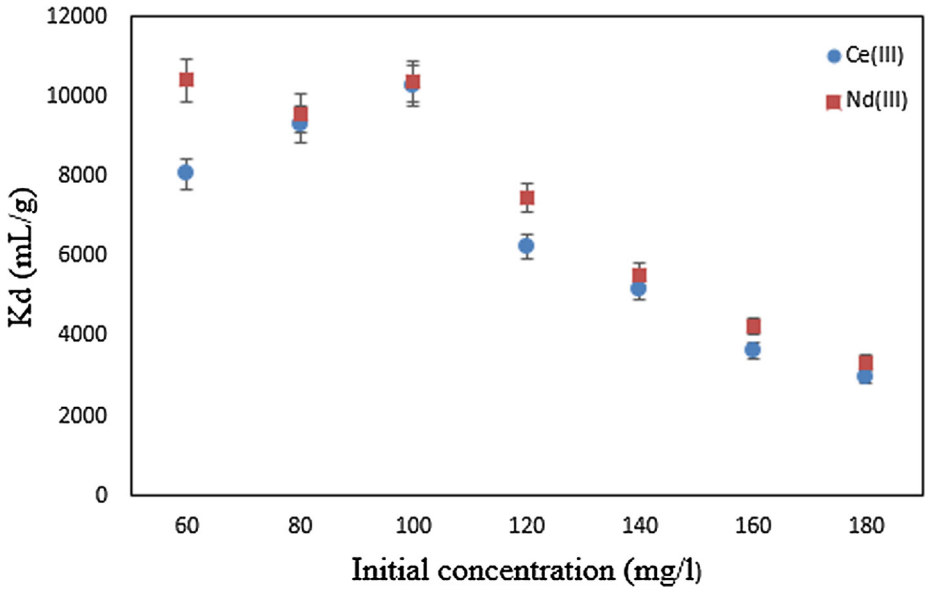

Fig. 8. Dependence of distribution coefficient (Kd) on initial concentration of Ce^{3+} or Nd^{3+} in the equilibrium adsorption study.

concentration is shown in Fig. 8 and the values are between ca. 10251 to 3000 mL/g and 10400 to 3300 mL/g for Ce^{3+} or Nd^{3+}, respectively. The high values of K_d represents more effective adsorbent for the separation of REEs [53]. For the PS-DGAnf studied, the Kd value is attributed to the chelation mechanism of diglycolic amic acid and the distribution coefficient values for Ce^{3+} or Nd^{3+} are higher or showed similar values to several studies reported in literature [10,54–56]. Demir et al, [28] reported a high Kd value ca. 30000 mL/g for Nd^{3+} at higher pH using carboxylic acid functionalized porous aromatic frameworks though the value dropped to below 20 at a lower pH. Roosen and Binnemans [46] also reported high Kd values for Nd^{3+} and Dy^{3+} at about 10000 mL/g with DTPA chitosan-based sorbents which dropped below 1000 mL/g at pH 2.

3.5. Effect of contact time

Another important parameter investigated was contact time which could be used for evaluating the adsorption kinetics. The result showed that the adsorption rate increased sharply within the first minute before the rate of adsorption slowed down gradually to attain the maximum equilibrium within 10 mins for Ce^{3+} and 20 min for Nd^{3+} ions as represented in Fig. 9. The fast adsorption rate during the first 10 min was associated with the high number of vacant surface sites of the nanofiber adsorbent available during the adsorption of the metal ions. Within the first 20 min, the amount adsorbed reached 119.4 mg g^{-1} Ce^{3+} and 108.4 mg g^{-1} Nd^{3+} of the available concentration of metal ions present in the solution. Hence, a contact time of 20 min was adequate to reach equilibrium for PS-DGAnf.

The high adsorption rate was attributed to low diffusional constraints as well as the high surface area and numerous binding sites of PS-DGAnf. After 20 mins, no further adsorption occurred on the adsorbent due to limited supply of metal ions in solution as more than 90% of the adsorbate was removed from solution. The short time required to attain equilibrium shows that the PS-DGAnf has a great potential and very high adsorption efficiency for Ce^{3+} or Nd^{3+} uptake when compared to other adsorbent surface modification using diglycolic-based selective ligands which reported fast metal binding kinetics toward REEs [10,15,57].

3.6. Desorption and reusability studies

The regeneration and desorption cycle of an adsorbent is crucial and essential for its possible practical application. The reusability of PS-DGAnf for Ce^{3+} or Nd^{3+} was studied by evaluating four consecutive cycles using 1 M HNO_3 solution as regenerant and the results are depicted in Fig. 10. The nanofibers retained high uptake capacity after the third and the fourth cycles of adsorption–desorption. PS-DGAnf maintained up to 92% capacity for the removal of Nd^{3+} after 4 cycles and was able to maintain capacity for Ce^{3+} uptake up to 96.7% of the initial concentration after four adsorption–desorption cycles. The key objective of the regeneration and desorption procedure was to reinstate the adsorption capacity of the used adsorbent and to recover valued metal ions existing in the adsorbed phase. These results compare favourably to the study by Galhoum et al. (2017) [34] which used nitric acid (0.5 M solution) as regenerant to desorb Nd^{3+} from loaded sorbents. Regeneration was carried out with 1 M HNO_3 to desorb the metal ions taken up on the adsorbent for reuse without disrupting the ligand attached. It was considered that the desorption by HNO_3 is caused by ion exchange reaction between protons and adsorbed ions and this stripping agent was earlier tested for ligand stability to confirm whether the functional fibers can withstand its short term contact (see FTIR spectra Fig. 3d).

3.7. Selective adsorption

Much attention for potential source of REE has been directed towards identifying and leveraging new or recycled sources of REE such as electronics waste, coal fly ash, brines, and various industrial wastes to meet surging demand [58–60]. To investigate the selectivity of the PS-DGAnf toward Ce^{3+}, the selective adsorption study was carried out in an aqueous solution containing mixed ions of Ce^{3+}, Co^{2+}, Ni^{2+} and Sr^{2+}. Similarly, the adsorption of the different metal ions in solutions of single ions using PS-DGAnf was also evaluated. The amount of every single metal ion sorbed onto the PS-DGAnf was calculated and the results are summarised in Table 3. The amount of Ce^{3+} adsorbed despite the existence of competing ions was 100.3 mg g^{-1}, which was only slightly lower than what was obtained in the single ion solution (119.4 mg g^{-1}). The selectivity was attributed to the low amount of competing adsorption of other different metal ions such as Co^{2+}, Ni^{2+} and Sr^{2+} present in solution which is suggested to have led to a small alteration in the Ce^{3+} adsorption equilibrium. The high selective adsorption coefficient revealed that the PS-DGAnf showed much higher selectivity toward Ce^{3+} in the modelled solution than to the other metals investigated. The PS-DGAnf depicted better adsorption selectivity toward

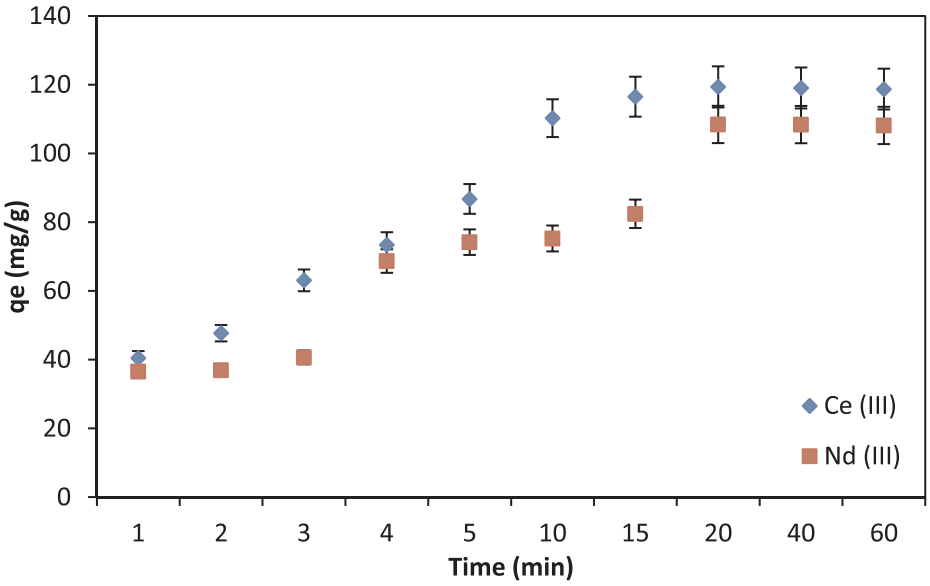

Fig. 9. The effect of contact in the time removal efficiency of (a) Ce^{3+} (b) Nd^{3+} from aqueous solution by PS-DGAnf (Ce^{3+} or Nd^{3+} concentration −100 mg/L; pH −6; adsorbent dosage −0.0075 g /10 mL).

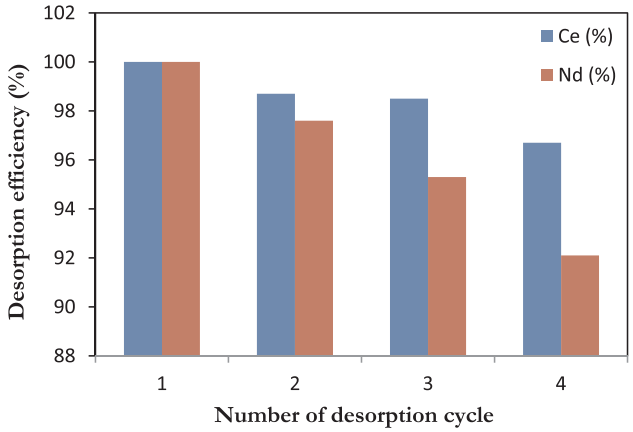

Fig. 10. Desorption efficiency for Ce^{3+} or Nd^{3+} from PS-DGAnf for three cycles of adsorption–desorption (initial concentration −100 mg/L; adsorbent dosage −0.0075 g/10 mL; stripping agent −1 M HNO_3; desorption time −60 min).

Table 3
Selectivity coefficients (S) and adsorption capacities of diverse metal ions in solution using PS-DGAnf (Contact time −200 rpm for 1 h; concentration −100 mg/L; pH −6; solution pH 6; adsorbent dosage −0.0075 g/10 mL).

Adsorption capacity, (mg g^{-1})	Co^{2+}	Ni^{2+}	Sr^{2+}	Ce^{3+}
Single solution	2.76	5.50	18.6	119.4
Mixed solution	2.01	4.99	3.30	100.3
Selectivity coefficient (S) (Ce/Co, Ni or Sr)	49.9	20.1	30.4	1

Ce^{3+} over other metal ions which may be related to the chelating bonding orbital and the ion radius of the different metal ions. The N_2 BET adsorption–desorption characterisation indicated a porous structure for the adsorbent and the surface area was large enough to result in a high adsorption rate compared to the pristine nanofiber adsorption (not shown). The high selectivity for the rare earth elements was therefore attributed to chelation by the tridentate diglycolic acid framework. PS-DGAnf containing diglycolic acid exhibit higher extraction of trivalent lanthanides such as Ce^{3+} compared to divalent metal ions and this finding solves the first major challenge for the REE industry, which is the separation of REEs from base metals [61]. The co-existence in solution of selected metal ions did not significantly interfere with the adsorption of REEs binding to PS-DGAnf as can be deduced from the high selectivity coefficient.

Ce^{3+} was selected for the experiments because both dynamic and equilibrium experiments indicated that the nanofiber adsorbents had very comparable sorption properties and capacities for the two REEs (Ce^{3+} and Nd^{3+}) signifying that a selective separation between different REEs may be challenging at the metal-binding equilibrium due to their close sorption capacities as shown previously in Table 1. Their individual differences were therefore not large enough and would therefore require more enrichment steps to achieve metal separation between these two REEs. The selective separation and extraction of dilute rare earth metal ions from solutions containing higher concentrations of base metal ions is necessary in the recovery process of rare earth elements from low grade ores and scrap. This adsorbent, PS-DGAnf, can therefore be useful for the recovery and separation of REEs from base metals.

4. Conclusions

A novel electrospun polystyrene diglycolic acid (PS-DGAnf) nanofiber adsorbent for the efficient and selective adsorption of Nd^{3+} and Ce^{3+} ions was prepared by electrospinning of PS nanofibers, which were chemically modified with diglycolic anhydride (DGA) via an electrophilic aromatic substitution of the ligand onto the PS nanofiber. The optimum polystyrene electrospinning conditions for the experiments were obtained under the operating conditions of concentration (15 wt%); voltage (20 kV); solution flow rate (0.8 mL/h) and collector distance of 17 cm. The advantages of the stable and selective ligand on the nanofiber and high DGA loading of 0.827 g g^{-1} with fast kinetics allowed the PS-DGAnf nanofiber to be applied as efficient and selective adsorbant of rare earth metals such as Ce^{3+} and Nd^{3+} ions. The electrospinning and modification of PS-DGAnf was confirmed by ATR-FTIR, HR-SEM, BET and TGA techniques. The kinetic study of PS-DGAnf showed that maximum equilibrium could be attained within 15 mins of the adsorption process. The adsorption at pH 6.0 of Ce^{3+} and Nd^{3+} ions with the maximum equilibrium uptake capacity of 152.5 mg g^{-1} (1.09 mmol/g) of Ce^{3+} and 146.2 mg g^{-1} (1.01 mmol/g) of Nd^{3+} respectively was well fitted to the Langmuir isotherm equation. Furthermore, the PS-DGAnf showed higher affinity toward trivalent Ce^{3+} than to other common divalent metal ions such as Co^{2+}, Ni^{2+} and

Sr^{2+}. This PS-DGAnf could be regenerated successfully and retained high uptake capacity in aqueous solution of 1 M HNO_3 with no significant loss of capacity after four successive cycles. The developed electrospun polystyrene diglycolic acid nanofiber adsorbents can be utilised for the rapid and selective recovery and separation of rare earth metals ions from base metals in aqueous solution.

Declaration of Competing Interest

The authors wish to confirm that there are no known conflicts of interest associated with this publication. Therefore, there are no competing interests to declare.

Acknowledgments

The study was supported by Environmental and Nano Sciences Research Group, University of the Western Cape, South Africa; Water Research Commission, South Africa (WRC K5//2391); Research Foundation of the Lappeenranta University of Technology; Academy of Finland; Finnish Cultural Foundation/South Karelia Regional fund and Magnus Ehrnrooth Foundation.

Appendix A. Supplementary material

Supplementary data to this article can be found online at https://doi.org/10.1016/j.seppur.2019.116059.

References

[1] S. Xu, S. Zhang, K. Chen, J. Han, H. Liu, K. Wu, Biosorption of La 3+ and Ce 3+ by Agrobacterium sp. HN1, J. Rare Earths. 29 (2011) 265–270.
[2] O. Pereao, C. Bode-Aluko, O. Fatoba, K. Laatikainen, L. Petrik, Rare earth elements removal techniques from water/wastewater: a review, Desalin. Water Treat. 130 (2018) 71–86, https://doi.org/10.5004/dwt.2018.22844.
[3] T. Sahu, S. Singh Bisht, K. Ranjan Das, S. Kerkar, Nanoceria: synthesis and biomedical applications, Curr. Nanosci. 9 (2013) 588–593.
[4] R.D. Abreu, C.A. Morais, Study on separation of heavy rare earth elements by solvent extraction with organophosphorus acids and amine reagents, Miner. Eng. 61 (2014) 82–87.
[5] C.A. Bode-Aluko, O. Pereao, G. Ndayambaje, L. Petrik, Adsorption of toxic metals on modified polyacrylonitrile nanofibres: a review, Water. Air. Soil Pollut. 228 (2017), https://doi.org/10.1007/s11270-016-3222-3.
[6] N. Van Nguyen, A. Iizuka, E. Shibata, T. Nakamura, Study of adsorption behavior of a new synthesized resin containing glycol amic acid group for separation of scandium from aqueous solutions, Hydrometallurgy. 165 (2016) 51–56.
[7] M.S. Gasser, M.I. Aly, Separation and recovery of rare earth elements from spent nickel–metal-hydride batteries using synthetic adsorbent, Int. J. Miner. Process. 121 (2013) 31–38.
[8] V. Korovin, Y. Shestak, Scandium extraction from hydrochloric acid media by Levextrel-type resins containing di-isooctyl methyl phosphonate, Hydrometallurgy. 95 (2009) 346–349.
[9] H. Naganawa, K. Shimojo, H. Mitamura, Y. Sugo, J. Noro, M. Goto, A new“ green” extractant of the diglycol amic acid type for lanthanides, Solvent Extr. Res. Dev. 14 (2007) 151–159.
[10] B.R. Selvan, K. Dasthaiah, A.S. Suneesh, K.A. Venkatesan, M.P. Antony, R.L. Gardas, Diglycolic acid modified zirconium phosphate and studies on the extraction of Am (III) and Eu (III) from dilute nitric acid medium, Radiochim. Acta. 105 (2017) 275–283.
[11] K. Shimojo, N. Aoyagi, T. Saito, H. Okamura, F. Kubota, M. Goto, H. Naganawa, Highly efficient extraction separation of lanthanides using a diglycolamic acid extractant, Anal. Sci. 30 (2014) 263–269.
[12] K. Sakaki, H. Sugahara, T. Kume, M. Ohashi, H. Naganawa, K. Shimojo, Method for synthesizing rare earth metal extractant-US Patent-US8841482B2, 2014.
[13] Y. Hosomomi, R. Wakabayashi, F. Kubota, N. Kamiya, M. Goto, Diglycolic amic acid-modified E. coli as a biosorbent for the recovery of rare earth elements, Biochem. Eng. J. 113 (2016) 102–106, https://doi.org/10.1016/J.BEJ.2016.06.005.
[14] R. Bai, F. Yang, Y. Zhang, Z. Zhao, Q. Liao, P. Chen, P. Zhao, W. Guo, C. Cai, Preparation of elastic diglycolamic-acid modified chitosan sponges and their application to recycling of rare-earth from waste phosphor powder, Carbohydr. Polym. 190 (2018) 255–261, https://doi.org/10.1016/J.CARBPOL.2018.02.059.
[15] T. Ogata, H. Narita, M. Tanaka, Adsorption behavior of rare earth elements on silica gel modified with diglycol amic acid, Hydrometallurgy. 152 (2015) 178–182, https://doi.org/10.1016/j.hydromet.2015.01.005.
[16] T. Ogata, H. Narita, M. Tanaka, Adsorption mechanism of rare earth elements by adsorbents with diglycolamic acid ligands, Hydrometallurgy. 163 (2016) 156–160.
[17] J. Fang, H. Niu, T. Lin, X. Wang, Applications of electrospun nanofibers, Chinese Sci. Bull. 53 (2008) 2265–2286.
[18] O. Pereao, C. Bode-Aluko, K. Laatikainen, A. Nechaev, L. Petrik, Morphology, modification and characterisation of electrospun polymer nanofiber adsorbent material used in metal ion removal, J. Polym. Environ. 27 (2019) 1843–1860, https://doi.org/10.1007/s10924-019-01497-w.
[19] M. Arslan, M. Yiğitoğlu, Use of methacrylic acid grafted poly (ethylene terephthalate) fibers for the removal of basic dyes from aqueous solutions, J. Appl. Polym. Sci. 110 (2008) 30–38.
[20] O.K. Pereao, C. Bode-Aluko, G. Ndayambaje, O. Fatoba, L.F. Petrik, Electrospinning: polymer nanofibre adsorbent applications for metal ion removal, J. Polym. Environ. 25 (2017) 1175–1189, https://doi.org/10.1007/s10924-016-0896-y.
[21] Y.J. Ryu, H.Y. Kim, K.H. Lee, H.C. Park, D.R. Lee, Transport properties of electrospun nylon 6 nonwoven mats, Eur. Polym. J. 39 (2003) 1883–1889, https://doi.org/10.1016/S0014-3057(03)00096-X.
[22] N. Bhardwaj, S.C. Kundu, Electrospinning: A fascinating fiber fabrication technique, Biotechnol. Adv. 28 (2010) 325–347, https://doi.org/10.1016/j.biotechadv.2010.01.004.
[23] S.D. Alexandratos, D.W. Crick, Polymer-supported reagents: Application to separation science, Ind. Eng. Chem. Res. 35 (1996) 635–644.
[24] A. Bahramzadeh, P. Zahedi, M. Abdouss, Acrylamide-plasma treated electrospun polystyrene nanofibrous adsorbents for cadmium and nickel ions removal from aqueous solutions, J. Appl. Polym. Sci. 133 (2016).
[25] E. Repo, J.K. Warchol, T.A. Kurniawan, M.E.T. Sillanpää, Adsorption of Co(II) and Ni(II) by EDTA- and/or DTPA-modified chitosan: Kinetic and equilibrium modeling, Chem. Eng. J. 161 (2010) 73–82, https://doi.org/10.1016/j.cej.2010.04.030.
[26] K. Teramoto, Y. Nakamoto, Amidomethylation of vinyl aromatic polymers with N-methylol-2-chloroacetamide, Polym. J. 34 (2002) 363–369.
[27] H.E. Zaugg, W.B. Martin, α-Amidoalkylations at Carbon, Org. React. John Wiley & Sons, Inc., 2011, pp. 52–269, , https://doi.org/10.1002/0471264180.or014.02.
[28] S. Demir, N.K. Brune, J.F. Van Humbeck, J.A. Mason, T.V. Plakhova, S. Wang, G. Tian, S.G. Minasian, T. Tyliszczak, T. Yaita, T. Kobayashi, S.N. Kalmykov, H. Shiwaku, D.K. Shuh, J.R. Long, Extraction of lanthanide and actinide ions from aqueous mixtures using a carboxylic acid-functionalized porous aromatic framework, ACS Cent. Sci. 2 (2016) 253–265, https://doi.org/10.1021/acscentsci.6b00066.
[29] E.-J. Lee, A.K. An, T. He, Y.C. Woo, H.K. Shon, Electrospun nanofiber membranes incorporating fluorosilane-coated TiO 2 nanocomposite for direct contact membrane distillation, J. Memb. Sci. 520 (2016) 145–154.
[30] J. Wu, A.K. An, J. Guo, E.-J. Lee, M.U. Farid, S. Jeong, CNTs reinforced superhydrophobic-oleophilic electrospun polystyrene oil sorbent for enhanced sorption capacity and reusability, Chem. Eng. J. 314 (2017) 526–536, https://doi.org/10.1016/j.cej.2016.12.010.
[31] G. Limousin, J.-P. Gaudet, L. Charlet, S. Szenknect, V. Barthès, M. Krimissa, Sorption isotherms: A review on physical bases, modeling and measurement, Appl. Geochemistry. 22 (2007) 249–275, https://doi.org/10.1016/J.APGEOCHEM.2006.09.010.
[32] Ricardo D. Andrade P.; Roberto Lemus M.; Carmen E. Pérez C., Models of Sorption Isotherms for Food: Uses and Limitations, Vitae. 18 (2011) 325–334. http://www.scielo.org.co/pdf/vitae/v18n3/v18n3a12.pdf (accessed February 8, 2019).
[33] A. Eser, V.N. Tirtom, T. Aydemir, S. Becerik, A. Dinçer, Removal of nickel (II) ions by histidine modified chitosan beads, Chem. Eng. J. 210 (2012) 590–596.
[34] A.A. Galhoum, K.M. Hassan, O.A. Desouky, A.M. Masoud, T. Akashi, Y. Sakai, E. Guibal, Aspartic acid grafting on cellulose and chitosan for enhanced Nd (III) sorption, React. Funct. Polym. 113 (2017) 13–22.
[35] M.R. Karim, M.O. Aijaz, N.H. Alharth, H.F. Alharbi, F.S. Al-Mubaddel, M.R. Awual, Composite nanofibers membranes of poly(vinyl alcohol)/chitosan for selective lead (II) and cadmium(II) ions removal from wastewater, Ecotoxicol. Environ. Saf. 169 (2019) 479–486, https://doi.org/10.1016/J.ECOENV.2018.11.049.
[36] M. Jiang, T. Han, J. Wang, L. Shao, C. Qi, X.M. Zhang, C. Liu, X. Liu, Removal of heavy metal chromium using cross-linked chitosan composite nanofiber mats, Int. J. Biol. Macromol. 120 (2018) 213–221, https://doi.org/10.1016/J.IJBIOMAC.2018.08.071.
[37] K.Y. Foo, B.H. Hameed, Insights into the modeling of adsorption isotherm systems, Chem. Eng. J. 156 (2010) 2–10.
[38] D. Sadovsky, A. Brenner, B. Astrachan, B. Asaf, R. Gonen, Biosorption potential of cerium ions using Spirulina biomass, J. Rare Earths. 34 (2016) 644–652.
[39] S. Yavarpour, S.H. Mousavi, M. Torab-Mostaedi, R. Davarkhah, H.G. Mobtaker, Effective removal of Ce (III) and Pb (II) by new hybrid nano-material: H n PMo 12 O 40@ Fe (III) x Sn (II) y Sn (IV) 1–x− y, Process Saf. Environ. Prot. 98 (2015) 211–220.
[40] Z. Shojaei, E. Iravani, M.A. Moosavian, M. Torab-Mostaedi, Removal of cerium from aqueous solutions by amino phosphate modified nano TiO2: kinetic, and equilibrium studies, Iran. J. Chem. Eng. 13 (2016).
[41] A.R. Elsalamouny, O.A. Desouky, S.A. Mohamed, A.A. Galhoum, E. Guibal, Uranium and neodymium biosorption using novel chelating polysaccharide, Int. J. Biol. Macromol. 104 (2017) 963–968.
[42] F. Wang, J. Zhao, X. Wei, F. Huo, W. Li, Q. Hu, H. Liu, Adsorption of rare earths (III) by calcium alginate–poly glutamic acid hybrid gels, J. Chem. Technol. Biotechnol. 89 (2014) 969–977.
[43] H.-J. Park, L.L. Tavlarides, Adsorption of neodymium (III) from aqueous solutions using a phosphorus functionalized adsorbent, Ind. Eng. Chem. Res. 49 (2010) 12567–12575.
[44] L. Zhang, D. Wu, B. Zhu, Y. Yang, L. Wang, Adsorption and selective separation of neodymium with magnetic alginate microcapsules containing the extractant 2-ethylhexyl phosphonic acid mono-2-ethylhexyl ester, J. Chem. Eng. Data. 56 (2011) 2280–2289.

[45] M. Najafi Lahiji, A.R. Keshtkar, M.A. Moosavian, Adsorption of cerium and lanthanum from aqueous solutions by chitosan/polyvinyl alcohol/3-mercaptopropyltrimethoxysilane beads in batch and fixed-bed systems, Part. Sci. Technol. (2016) 1–11.
[46] J. Roosen, K. Binnemans, Adsorption and chromatographic separation of rare earths with EDTA- and DTPA-functionalized chitosan biopolymers, J. Mater. Chem. A. 2 (2014) 1530–1540, https://doi.org/10.1039/c3ta14622g.
[47] D. Saha, S.D. Akkoyunlu, R. Thorpe, D.K. Hensley, J. Chen, Adsorptive recovery of neodymium and dysprosium in phosphorous functionalized nanoporous carbon, J. Environ. Chem. Eng. 5 (2017) 4684–4692, https://doi.org/10.1016/J.JECE.2017.09.009.
[48] M.R. Awual, M.M. Hasan, A. Shahat, M. Naushad, H. Shiwaku, T. Yaita, Investigation of ligand immobilized nano-composite adsorbent for efficient cerium (III) detection and recovery, Chem. Eng. J. 265 (2015) 210–218.
[49] Y. Sasaki, P. Rapold, M. Arisaka, M. Hirata, T. Kimura, C. Hill, G. Cote, An additional insight into the correlation between the distribution ratios and the aqueous acidity of the TODGA system, Solvent Extr. Ion Exch. 25 (2007) 187–204.
[50] K. Matloka, A. Gelis, M. Regalbuto, G. Vandegrift, M.J. Scott, Highly efficient binding of trivalent f-elements from acidic media with a C 3-symmetric tripodal ligand containing diglycolamide arms, Dalt. Trans. (2005) 3719–3721.
[51] J. Florek, A. Mushtaq, D. Larivière, G. Cantin, F.-G. Fontaine, F. Kleitz, Selective recovery of rare earth elements using chelating ligands grafted on mesoporous surfaces, RSC Adv. 5 (2015) 103782–103789.
[52] J. Florek, S. Giret, E. Juère, D. Larivière, F. Kleitz, Functionalization of mesoporous materials for lanthanide and actinide extraction, Dalt. Trans. 45 (2016) 14832–14854, https://doi.org/10.1039/C6DT00474A.
[53] X. Zheng, E. Liu, F. Zhang, Y. Yan, J. Pan, Efficient adsorption and separation of dysprosium from NdFeB magnets in an acidic system by ion imprinted mesoporous silica sealed in a dialysis bag, Green Chem. 18 (2016) 5031–5040, https://doi.org/10.1039/C6GC01426G.
[54] S. Ravi, Y.-R. Lee, K. Yu, J.-W. Ahn, W.-S. Ahn, Benzene triamido-tetraphosphonic acid immobilized on mesoporous silica for adsorption of Nd3+ ions in aqueous solution, Microporous Mesoporous Mater. 258 (2018) 62–71, https://doi.org/10.1016/J.MICROMESO.2017.09.006.
[55] H. Moriwaki, R. Masuda, Y. Yamazaki, K. Horiuchi, M. Miyashita, J. Kasahara, T. Tanaka, H. Yamamoto, Application of freeze-dried powders of genetically engineered microbial strains as adsorbents for rare earth metal ions, ACS Appl. Mater. Interfaces. 8 (2016) 26524–26531, https://doi.org/10.1021/acsami.6b08369.
[56] J. Florek, F. Chalifour, F. Bilodeau, D. Larivière, F. Kleitz, Nanostructured hybrid materials for the selective recovery and enrichment of rare earth elements, Adv. Funct. Mater. 24 (2014) 2668–2676, https://doi.org/10.1002/adfm.201303602.
[57] L.L. Perreault, S. Giret, M. Gagnon, J. Florek, D. Larivière, F. Kleitz, Functionalization of mesoporous carbon materials for selective separation of lanthanides under acidic conditions, ACS Appl. Mater. Interfaces. 9 (2017) 12003–12012, https://doi.org/10.1021/acsami.6b16650.
[58] X.-H. Fang, F. Fang, C.-H. Lu, L. Zheng, Removal of Cs+, Sr2+, and Co2+ Ions from the mixture of organics and suspended solids aqueous solutions by zeolites, Nucl. Eng. Technol. 49 (2017) 556–561, https://doi.org/10.1016/J.NET.2016.11.008.
[59] P. Zhang, Y. Wang, D. Zhang, Removal of Nd(III), Sr(II), and Rb(I) Ions from aqueous solution by thiacalixarene-functionalized graphene oxide composite as an adsorbent, J. Chem. Eng. Data. 61 (2016) 3679–3691, https://doi.org/10.1021/acs.jced.6b00622.
[60] J.C. Callura, K.M. Perkins, C.W. Noack, N.R. Washburn, D.A. Dzombak, A.K. Karamalidis, Selective adsorption of rare earth elements onto functionalized silica particles, Green Chem. 20 (2018) 1515–1526, https://doi.org/10.1039/C8GC00051D.
[61] N. Sui, K. Huang, C. Zhang, N. Wang, F. Wang, H. Liu, Light, middle, and heavy rare-earth group separation: a new approach via a liquid–liquid–liquid three-phase system, Ind. Eng. Chem. Res. 52 (2013) 5997–6008.